A DUAL-BAND WLAN/UWB PRINTED WIDE SLOT ANTENNA FOR MIMO/ DIVERSITY APPLICATIONS

Sajad Mohammad, ali nezhad, Hamid Reza Hassani, and Ali Foudazi
Department of Electrical and Electronic Engineering, Shahed University, Tehran, Iran; Corresponding author: hassani@shahed.ac.ir

Received 10 June 2012

ABSTRACT: *In this article, a dual-band WLAN/ultrawideband (UWB) printed wide slot microstrip-fed antenna is presented for multi-input multi-output (MIMO)/diversity applications. The proposed antenna consists of a U-shaped patch, a T-shaped monopole path, and a pentagonal wide slot in the ground plane. The antenna is designed to cover both the WLAN (2.4–2.485 GHz) and UWB (3.1–10.6 GHz) ranges, with value of S_{11} below −10 dB. The antenna is constructed on a FR4 substrate with overall dimensions of 28 × 28 × 1 mm^3. It is shown that the proposed dual-band antenna is suitable for diversity polarization applications. The simulation results show that the different configurations of the antenna in the MIMO/diversity have good S-parameters over the operating frequency bands. The simulation and measured results of the proposed dual-band antenna as well as that of the MIMO/diversity antenna configuration agree well.* © 2012 Wiley Periodicals, Inc. Microwave Opt Technol Lett 54:461–465, 2013; View this article online at wileyonlinelibrary.com. DOI 10.1002/mop.27391

Key words: *ultrawideband antenna; monopole antenna; multi-input multi-output; diversity*

1. INTRODUCTION

Multi-Input Multi-Output (MIMO) communication systems due to their ability to reduce multipath fading and increased channel capacity are of importance in wireless communication systems. Ultrawideband (UWB) MIMO communication systems can further increases the capacity of channel in comparison with narrowband MIMO systems [1]. From a MIMO antenna array one requires features, such as compact structure, high radiation efficiency, low envelope correlation, and high isolation between the signal ports [2]. To achieve maximum channel capacity, the array with high gain and wide lobe pattern is required [3].

An important element in a MIMO/diversity system is the antenna structure. The printed antennas are strongly favored for their attractive features of low cost, easy fabrication, and their capability of integration with small terminal devices [3–7].

To design a UWB MIMO/diversity antenna, the mutual coupling between antenna elements should be low. Several techniques have been used in the literature to improve the isolation characteristics between the elements. Common to all these techniques is the use of external slits/strips in between the array elements. By inserting slits in the ground plane of the structure, isolation is improved [4]. By introducing protruding strips in the ground plane in between the array elements mutual coupling can be reduced, [5, 6].

Printed monopole wide slot antennas can be more desirable as they can provide higher gain in comparison with printed monopole antennas. Design of a UWB antenna, using different shapes of printed microstrip-fed wide slot antenna is presented in Refs. 8 and 9. To obtain a multiband printed antenna which also includes the UWB range, Ref. 10has used an L-shaped resonant element at the corner of a UWB printed monopole antenna. This integrates the Bluetooth band with the existing UWB band and the overall dimension of antenna is 42 × 48 × 1 mm^3.

In this article, a new printed wide slot antenna configuration suitable for the design of a multiband MIMO/diversity antenna that includes the UWB range and an extra band below the UWB range is presented. Unlike the previously reported methods, in the new design there is no need for any external slits/strips. Different MIMO antenna array configurations are considered and *S*-parameter results are provided. The simulations are carried out using the commercially available software package HFSS and results are compared with those of measurement.

2. ANTENNA DESIGN

To have a UWB diversity antenna, the antenna element should be designed in such a way that it has high gain, wide lobe pattern, and low mutual coupling. Printed UWB monopole antennas are able to provide a wide lobe pattern (omnidirectional), whereas printed wide slot antennas, due to their larger ground plane, can also provide a higher gain. In the printed slot antennas, there is a slot within the ground plane unlike the case of a monopole antenna with limited ground at the bottom of the structure. The presence of the ground edges in the slot can lead to a better reduction in mutual coupling when an array is formed as compared to that of a monopole structure. Thus, in this work, a printed wide slot antenna is used [11].

To design a UWB printed wide slot antenna, the structure of Figure 1 is considered which is simple and has a few parameters. The dimension of the antenna is 28 × 28 × 1 mm^3 and is fabricated on FR4 substrate with effective permittivity of 4.4 and loss tangent of 0.02. A simple pentagonal slot in the ground plane is used to obtain omnidirectional radiation pattern and wide impedance bandwidth. The slot is fed by a simple rectangular patch in which a half ellipse is removed, leading to a tapered U-shaped patch. The radius of the ellipse in the *x*- and *y*-directions is set at 5 and 8 mm, respectively. The patch is fed by a feed line of width fixed at 1.86 mm that provides 50 Ω input impedance.

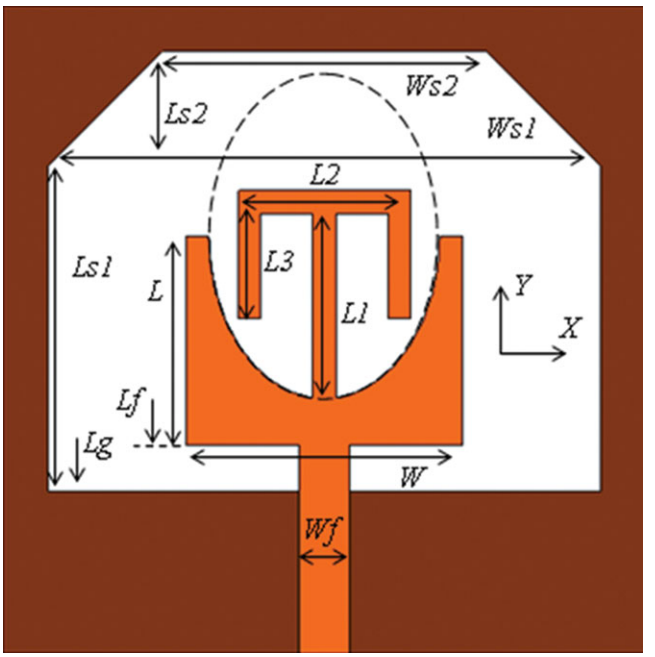

Figure 1 Printed planar slot antenna with UWB/WLAN bands. [Color figure can be viewed in the online issue, which is available at wileyonlinelibrary.com]

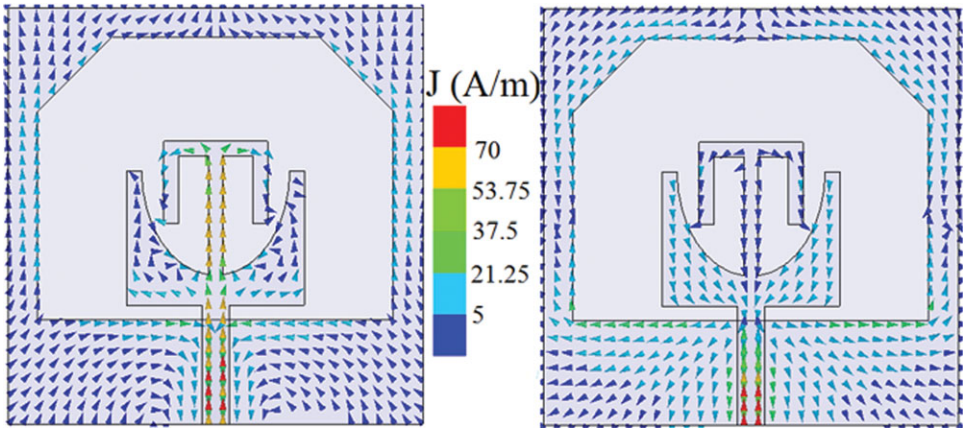

Figure 2 Current distributions on the proposed dual-band antenna at (a) 2.4 and (b) 7 GHz frequencies. [Color figure can be viewed in the online issue, which is available at wileyonlinelibrary.com]

To create an extra band below the UWB range, a quarter-wavelength long strip should be added to the initial U-shaped patch. Generally, it is desired that the overall dimensions of dual-band antenna to be kept fix. Equation (1) shows the general formula to design a resonance strip in printed wide slot antennas.

$$L_{\text{total}} \approx \frac{\lambda_g}{4\sqrt{\frac{\varepsilon_r+1}{2}}} \tag{1}$$

To create the extra resonance band and cover the WLAN band, a T-shaped resonance strip is added to the base U-shaped patch, as shown in Figure 1. The T-shaped strip is chosen to make the structure symmetrical and keep the size of the strip compact. For dual-band operation, the total length of the resonance path is given by the following equation

$$L_{\text{total}} = L1 + L2/2 + L3 \tag{2}$$

The current distribution on the proposed WLAN/UWB antenna structure at 2.4 and 7 GHz frequencies are presented in Figures 2(a) and 2(b). As shown in Figure 2(a), at 2.4 GHz frequency, the U-shaped patch is inactive with negligible current while on the added T-shaped strip maximum current is seen at the beginning and minimum current at the end of the path. This verifies that the length of the strip is about quarter wavelength. Figure 2(b) at 7 GHz frequency shows that most of the current is on the patch and the added T-shaped strip has no effect on the U-shaped patch.

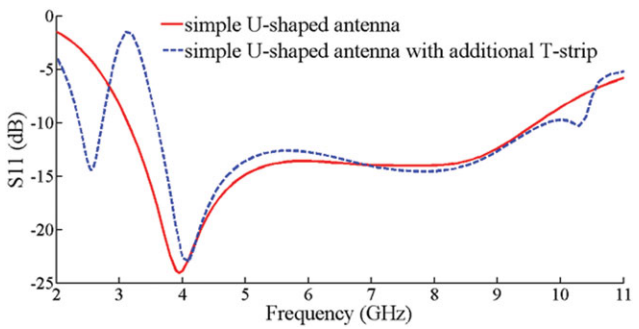

Figure 3 Simulated reflection coefficient of the proposed dual-band antenna with and without the T-shaped strip. [Color figure can be viewed in the online issue, which is available at wileyonlinelibrary.com]

The optimized parameters of the proposed dual-band antenna are as follows: $W = 12$ mm, $W_{s1} = 24$ mm, $W_{s2} = 14$ mm, $L_f = 8$ mm, $L_g = 7$ mm, $L = 9$ mm, $L_{s1} = 14$ mm, $L_{s2} = 5$ mm, $L_1 = 9$ mm, $L_2 = 7$ mm, $L_3 = 4.5$ mm.

3. RESULTS

The simulated reflection coefficient of the printed slot antenna with and without the T-shaped strip is shown in Figure 3. It is

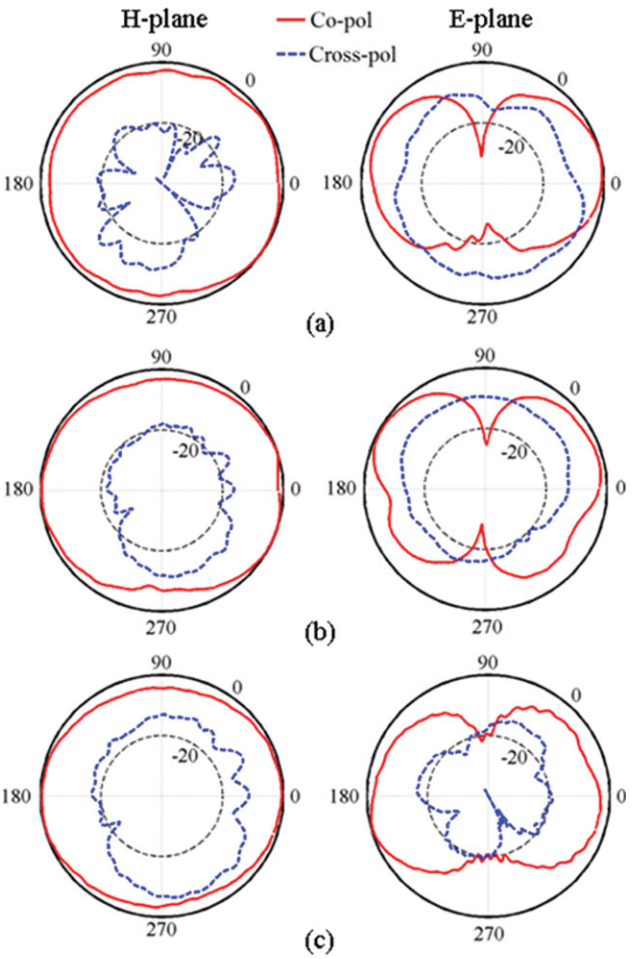

Figure 4 Measured *E*- and *H*-plane radiation patterns of the proposed dual-band antenna at (a) 2.4, (b) 4, and (c) 7 GHz. [Color figure can be viewed in the online issue, which is available at wileyonlinelibrary.com]

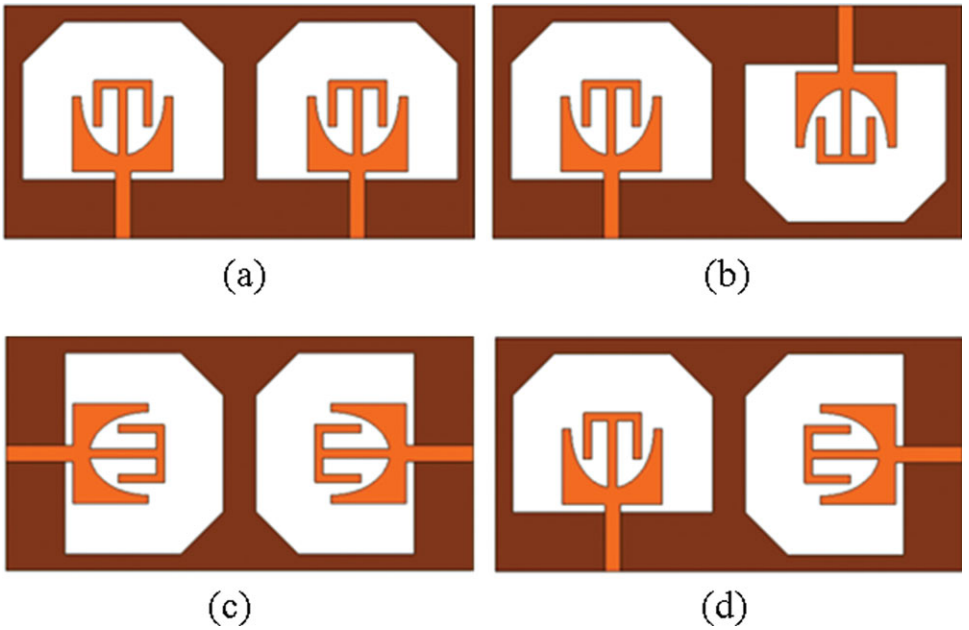

Figure 5 MIMO/diversity dual-band configurations (a) side by side, (b) parallel, (c) front-to-front, and (d) orthogonal. [Color figure can be viewed in the online issue, which is available at wileyonlinelibrary.com]

seen that the U-shaped antenna without the T-shaped strip operates over the UWB range of 3.1–10.6 GHz. The results of Figure 3 also show that the addition of the T-shaped strip results in a resonance band over 2.4–2.6 GHz. It can be seen that the added strip has negligible effect on the UWB range behavior. Thus, the proposed dual-band antenna covers the WLAN and the UWB ranges.

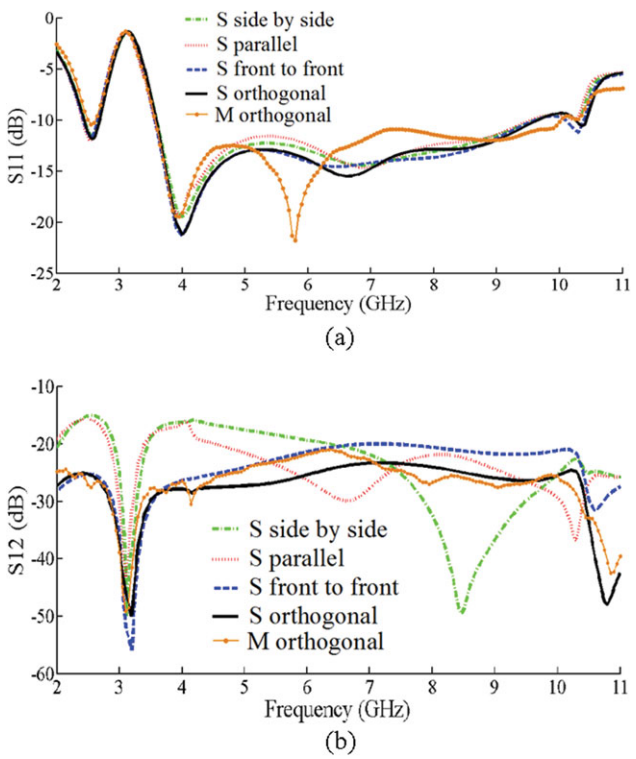

Figure 6 Simulated and measured *S*-parameters of MIMO/diversity dual-band configurations (a) S_{11} and (b) S_{12}. [Color figure can be viewed in the online issue, which is available at wileyonlinelibrary.com]

The measured copolarization and cross-polarization radiation patterns of the proposed WLAN/UWB antenna at 2.4, 4, and 7 GHz frequencies in both *E*- and *H*-planes are presented in Figure 4. As shown, the dual-band printed wide slot antenna has good and stable radiation characteristics in both planes.

4. MIMO/DIVERSITY CONFIGURATION

The proposed printed wide slot antenna that covers the WLAN and UWB ranges can be used for MIMO/diversity applications as it has good directive current distribution and can provide good isolation once placed in an array. Figure 5 shows four common configurations of the combination of two such antennas.

The simulated *S*-parameters of the MIMO/diversity configurations are shown in Figure 6. As can be seen, the proposed antenna provides good impedance matching with slight variation and high isolation between the two antenna ports without the usage of any external slot/slit. It is seen that in the orthogonal configuration, the value of S_{12} is completely below the -25 dB while in the other configurations the S_{12} goes above the -25 dB.

The envelope correlation ρ_e of the array configuration can be determined through the use of the *S*-parameters and is given in the following [3].

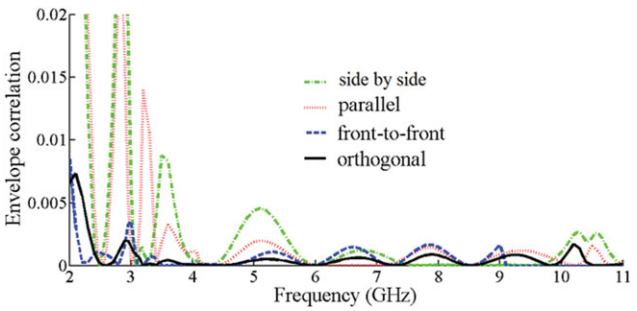

Figure 7 Simulated envelope correlation of the MIMO/diversity dual-band configurations of Figure 5. [Color figure can be viewed in the online issue, which is available at wileyonlinelibrary.com]

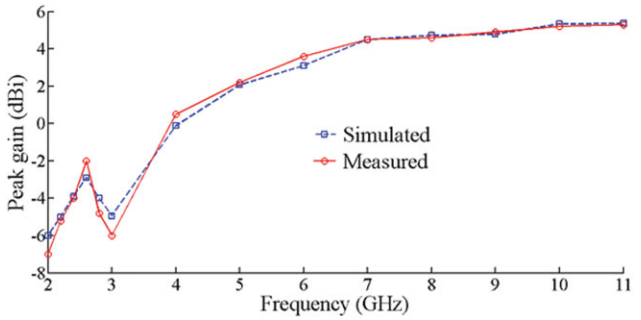

Figure 8 Simulated and measured peak gain of orthogonal MIMO/diversity dual-band slot monopole antenna. [Color figure can be viewed in the online issue, which is available at wileyonlinelibrary.com]

$$\rho_e = \frac{\left|S_{11}^* S_{21} + S_{12}^* S_{22}\right|^2}{\left|\left(1 - |S_{11}|^2 - |S_{21}|^2\right)\left(1 - |S_{22}|^2 - |S_{12}|^2\right)\right|} \tag{3}$$

The simulated envelope correlation of the proposed MIMO/diversity dual-band configuration of the array structures shown in Figure 5 is shown in Figure 7. It is noticed that all four configurations of the arrays provide less than 0.01 envelope correlations. This is well below the value of 0.3 that is acceptable [3].

Different configurations of the array of the printed wide slot antenna of Figure 5 produce acceptable *S*-parameters and envelope correlation results for diversity applications. The antenna array of Figure 5(d) has been fabricated and the measured results of *S*-parameters, peak gain, and efficiency are obtained. The measured results of *S*-parameters are shown in Figures 6 and Figure 8 shows the simulated peak gain. The peak gain over the WLAN and UWB bands varies from −2 to 5.5 dBi. The measured radiation efficiency is shown in Figure 9.

The radiation efficiency is obtained by calculating the ratio of the total radiated power of the array antenna to the total input power. For all frequency ranges, the radiation efficiency is between 85–95%.

The measured *E*- and *H*-plane radiation patterns of the array structure of Figure 5(d), for both copolarization and cross-polarization components at 2.4, 4, and 7 GHz are shown in Figure 10. It is noticed that the *H*-plane pattern is omnidirectional and has lower than −10 dB cross-polarization over all the frequency range. Also, the *E*-plane pattern is very stable with changes in frequency.

The low envelope correlation shown in Figure 7, the good isolation shown in Figure 6(b), and the good omnidirectional radiation patterns shown in Figure 10 confirm that the proposed printed wide slot antenna of Figure 1 is a good candidate for MIMO/diversity applications in WLAN/UWB ranges.

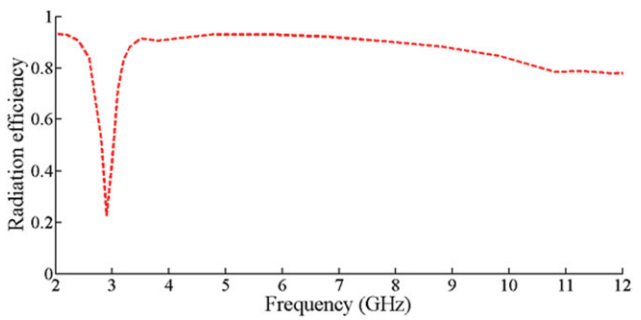

Figure 9 Measured radiation efficiency of orthogonal MIMO/diversity dual-band slot monopole antenna. [Color figure can be viewed in the online issue, which is available at wileyonlinelibrary.com]

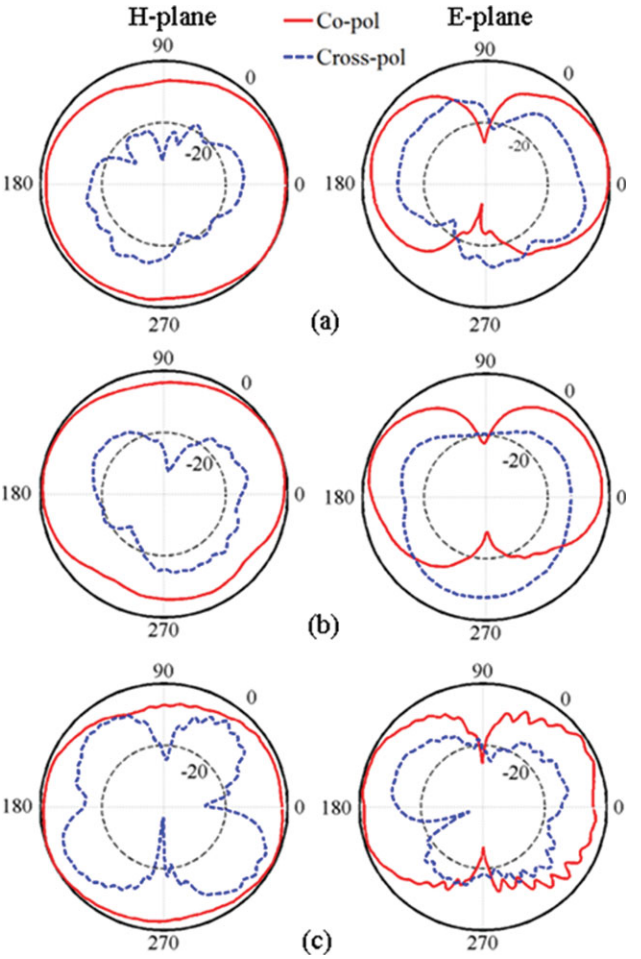

Figure 10 Measured *E*- and *H*-plane radiation patterns of the MIMO/diversity structure shown in Figures 5(d) at (a) 2.4, (b) 4, and (c) 7 GHz. [Color figure can be viewed in the online issue, which is available at wileyonlinelibrary.com]

5. CONCLUSION

In this article, a new printed wide slot antenna structure is presented that provides dual-band operation over the 2.4 GHz WLAN band and 3.16–10.6 GHz UWB range. The antenna is suitable for use in MIMO/diversity configurations. Four different configurations of the array of such two elements have been considered and the results for the orthogonal configuration shows low mutual coupling, low envelope correlation, good radiation efficiency between 85 and95%, acceptable antenna peak gain, and stable radiation pattern over various frequencies within the bandwidth.

REFERENCES

1. V.P. Tran and A. Sibille, Spatial multiplexing in UWB MIMO communications, Electron Lett 42 (2006), 931–932.
2. M.P. Karaboikis, V.C. Papamicheal, G.F. Tsachtsiris, C.F. Soras, andV.T. Makios, Integrating compact printed antennas onto small Diversity/MIMO terminals, IEEE Trans Antennas Propag 56 (2008), 2067–2078.
3. S.M.A. Nezhad and H.R. Hassani, A novel triband E-shaped printed monopole antenna for MIMO application, IEEE Antennas Wireless Propag Lett 9 (2010), 576–579.

4. H. Lee, J. Xiong, and S. He, A compact planar MIMO antenna system of four elements with similar radiation characteristics and isolation structure, IEEE Antennas Wireless Propag Lett 8 (2009), 1107–1110.
5. T.S.P. See, Z.N. Chen, and X. Qing, An ultrawideband diversity antenna, IEEE Trans Antennas Propag 57 (2009), 1279–1282.
6. S. Zhang, Z. Ying, J. Xiong, and S. He, Ultrawideband MIMO/diversity antennas with a tree-like structure to enhance wideband isolation, IEEE Antennas Wireless Propag Lett 7 (2009), 1107–1110.
7. A. Foudazi, A.R. Mallahzadeh, and S.M.A. Nezhad, A triple-band WLAN/WiMAX printed monopole antenna for MIMO applications, Microwave Opt Technol lett 54 (2012), 1321–1325.
8. S. Cheng, P. Hallbjörner, and A. Rydberg, Printed slot planar inverted cone antenna for ultrawideband applications, IEEE Antennas Wireless Propag Lett 7 (2008), 18–21.
9. A. Dastranj, A. Imani, and M. Naser-Moghadassi, Printed wide-slot antenna for wideband applications, IEEE Trans Antennas Propag 56 (2008), 3097–3102.
10. B.S. Yildirim, B.A. Cetiner, G. Roquetra, and L. Jofre, Integrated bluetooth and UWB antenna, IEEE Antennas Wireless Propag Lett 8 (2009), 149–152.
11. A. Foudazi, H.R. Hassani, and S.M.A. Nezhad, A dual-band WLAN/UWB printed wide slot antenna, In: IEEE Loughborough Antennas and Propagation Conference (LAPC), 2011.

MILLIMETER-WAVE PHASE SHIFTER BASED ON WAVEGUIDE-MOUNTED RF-MEMS

Dimitra Psychogiou,[1] Yunjia Li,[2] Jan Hesselbarth,[3] Stephane Kühne,[2] Dimitrios Peroulis,[4] Christofer Hierold,[2] and Christian Hafner[1]

[1] Laboratory for Electromagnetic Fields and Microwave Electronics, Department of Information Technology and Electrical Engineering, ETH Zurich, 8092 Zürich, Switzerland; Corresponding author: pdimitra@ifh.ee.ethz.ch

[2] Group of Micro and Nanosystems, Department of Mechanical and Process Engineering, ETH Zurich, 8092 Zürich, Switzerland

[3] Institute of Radio Frequency Technology, University of Stuttgart, Stuttgart 70569, Germany

[4] Birck Nanotechnology Center, School of Electrical and Computer Engineering, Purdue University, West Lafayette, IN 47907

Received 11 June 2012

ABSTRACT: *A continuously variable transmission type W-band phase shifter based on a single pole bandpass filter tuned by MEMS actuated fingers is reported. Tuning is achieved by means of two half-wavelength long conductive fingers that synchronously rotate upwards in an antiparallel fashion. The fingers deflection results in a distributed variable shunt capacitance which in turn leads to a variable analog phase shift. For an applied DC bias voltage between 0 and 26 V, the transmission phase can be continuously varied up to 46.4° at a frequency of 106 GHz with an insertion loss of less than 3.4 dB.* © 2012 Wiley Periodicals, Inc. Microwave Opt Technol Lett 54:465–468, 2013; View this article online at wileyonlinelibrary.com. DOI 10.1002/mop.27390

Key words: *phase shifter; RF-MEMS; resonator; analog tuning*

1. INTRODUCTION

Recent advances in imaging, radar and sensing systems have imposed the design of low loss, high-performing phase shifters for frequencies between 75 and 110 GHz commonly known as W-band. Millimeter-wave phase shifters are fundamental components of beamforming and phased antenna arrays intended to be used for automotive anticollision radar, weather monitoring, and medical imaging applications.

Topologies presented in the literature are mainly based on MEMS-switched true-time delay-lines or periodically capacitive-loaded transmission lines [1, 2]. In an alternative way, materials with tunable characteristics such as ferrites or ferroelectrics are used [3]. The first approach is often suitable for applications that require discrete phase shift variations. It requires a large number of tuning elements and is limited by high dissipation loss and low power handling. The second approach leads to bulky devices prone to excessive dissipated power due to the high dielectric losses of the involved materials and requires high power for operation.

For frequencies beyond a few GHz, air-filled metal waveguides outperform planar transmission lines in terms of low loss and high-power handling [4]. If used in combination with tunable components such as MEMS, they may pave the way to outperforming reconfigurable devices. An example of this approach was shown in Ref. 5 where a MEMS-based high impedance surface was used as a tunable back-short of a reflective-type phase shifter.

In this article, an analog transmission-type phase shifter based on MEMS tilting fingers [6] integrated beneath a half-wavelength long ridge waveguide resonator is presented. A prototype for frequencies between 96 and 106 GHz has been designed, manufactured, and experimentally validated.

2. PHASE SHIFTER CONCEPT

The proposed phase shifter concept is based on a single pole bandpass filter tuned around its center frequency by a single distributed shunt capacitance which results in a variation of the transmission phase. The maximum achievable phase shift is limited by the available variation of the capacitive loading and by the deterioration of the input reflection occurring at both minimum and maximum loading states. A realization concept of the phase shifter includes a low-impedance half-wavelength long ridge waveguide section and a MEMS chip with a pair of electrostatically actuated fingers, mounted inside the waveguide bottom wall (Fig. 1). The two sets of conductive fingers are either set flat in parallel with the waveguide bottom wall or synchronously rotate in an antiparallel fashion out of the bottom wall plane and toward the ridge (Fig. 2). Considering the length of the fingers of almost half a guided wavelength long, this rotational movement realizes a variable distributed shunt capacitance in the waveguide. For a design frequency around 100 GHz, the cross-sectional dimensions of the waveguide are: width: 1.5 mm, height: 1 mm, ridge width: 0.6 mm, ridge height: 0.5 mm. The low-impedance ridge has a height of 0.8 mm and the dimensions of the MEMS fingers are: length 1.4 mm and width 0.15 and 0.3 mm for the center finger and the edge fingers, respectively.

3. RF-MEMS CHIP

For the RF-MEMS chip design, a tilting micromirror approach is followed (Fig. 3). It is based on electrostatic actuation and features a torsional out-of-plane-modus of movement. Basic design and technology aspects have been presented in Ref. 7 and modified for the particular application. To achieve the high static deflection angle between 0 and 7.5° (g: 0–168 μm, h: 200–32 μm) with a low DC actuation voltage (<27.5 V), a soft SU8 polymer spring has been integrated underneath each torsional bar. The fabrication process is based on a bulk silicon micromachining process as described in Ref. 7. The chip is composed of a stack of three double-side polished monocrystalline silicon wafers (thickness: device layer 80 μm, stator layer